Friction **11**(9): 1708–1723 (2023)
https://doi.org/10.1007/s40544-022-0690-x
ISSN 2223-7690
CN 10-1237/TH
RESEARCH ARTICLE

Metastable hybridized structure transformation in amorphous carbon films during friction—A study combining experiments and MD simulation

Yefei ZHOU[1,2,3], Zhihao CHEN[1], Tao ZHANG[1], Silong ZHANG[2], Xiaolei XING[1,2,*], Qingxiang YANG[2], Dongyang LI[3,*]

[1] *School of Mechanical Engineering, Yanshan University, Qinhuangdao 066004, China*

[2] *State Key Laboratory of Metastable Materials Science & Technology, Yanshan University, Qinhuangdao 066004, China*

[3] *Chemical and Materials Engineering Department, University of Alberta, Edmonton T6G 2H5, Canada*

Received: 20 May 2022 / Revised: 27 July 2022 / Accepted: 04 September 2022

© The author(s) 2022.

Abstract: Amorphous carbon films have attracted substantial interest due to their exceptional mechanical and tribological properties. Previous studies revealed that the amorphous carbon films exhibited lower coefficient of friction (COF) because of the transformation in bond structure from sp^3-C to sp^2-C during friction processes. However, the mechanism for such a transformation during friction is not well understood. This study is conducted to get an insight into the metastable transformation in amorphous carbon film during friction by means of experiments and molecular dynamics (MD) simulation. Relevant wear tests showed that wear of the film changed from an abrasive wear mode to a mixture of abrasion and adhesive wear, resulting in a decrease in growth rate of the wear rate after the running-in stage. It is worth noting that the sp^3-C atoms were increased during the running-in stage when the films contained lower sp^3/sp^2 ratios. However, the formed sp^3-C atoms could only be short-lived and gradually transformed to sp^2-C atoms with the graphitization generated on the wearing surface of the films. The radial distribution function and translational order parameter indicated that the films' high sp^3/sp^2 ratio led to an increased sp^2-C proportion on the wear scar after friction, which caused an increased structural ordering.

Keywords: amorphous carbon film; metastable transformation; structural order; molecular dynamics (MD) simulation; tribological performance

1 Introduction

Friction and wear in dynamic mechanical systems can cause significant energy consumption [1]. Application of low-friction and wear-resistant films and coatings is an effective approach to reduce the energy consumption and mitigate wear issues. However, during friction and wear, the structure of the films or coatings could change, thus influencing the expected performance of the films/coatings. Therefore, understanding the materials' stability and response to friction and wear would help achieve better tribological control. The relationship between microstructure and tribological performance largely governs the design and application of the film/coating materials [2]. As a superior solid lubricant, amorphous carbon film has attracted intensive research attention for dynamic mechanical components in both microelectromechanical devices and traditional mechanical transmissions [3]. There are several types of amorphous carbon films, such as diamond-like carbon (DLC) films [4], graphite-like carbon (GLC)

* Corresponding authors: Xiaolei XING, E-mail: x.xing@ysu.edu.cn; Dongyang LI, E-mail: dongyang.li@ualberta.ca

films [5], fullerene-like carbon (FLC) films [6], onion-like carbon (OLC) [7], and similar films with hydrogen or metals doping, which have been synthesized over years [8].

Previous experiments and theoretical studies have shown that the tribological performance of amorphous carbon films may be quantitatively related to the state of chemisorption passivation of dangling bonds [9], graphitization [10], and transfer film [11] of the sliding interface, which are influenced by the environment, friction conditions, and properties of the materials and their counterparts [12]. Erdemir et al. [13] observed the desorption of the surface adsorbate of amorphous carbon films due to the frictional heat, causing exposure of the σ bond on surface and the formation of a strong covalent bond with the material at the contacting interface in an inert atmosphere or vacuum, which showed a high friction coefficient during the friction process. Wang et al. [14] studied the interfacial phase transformation of hydrogen-free DLC films during friction via MD simulation; they considered that lubrication of the films originated from the shear-induced strain localization, in which phase transition started by the local shear, resulting in a weakening of the shear force and thus lowered coefficient of friction (COF). Liu et al. [15] investigated the tribological performances of DLC films against various counterparts, and concluded that a transfer film with low shear strength could be generated between the film and the counterpart during the friction process, thus reducing COF and corresponding wear rate. Fan et al. [16] studied the stick–slip friction of the sp^2 nanocrystallited carbon films via *in-situ* transmission electron microscope (TEM) and nanofriction tests and revealed that the shear stress gradually increased with the contact load until reaching a critical shear strength at which the interfacial adhesion or bonding was broken in the stick stage. Chen [17] characterized the contact area produced on several a-C:H films and their counterpart via the scanning electron transmission microscopy and electron energy-loss spectroscopy; this study suggested that the occurrence of a super-lubricious state of the films was generally dependent on the formation of a tribolayer with interfacial nanostructures by different carbon rehybridization pathways due to the shear-induced phase transformation from sp^3-C to sp^2-C.

However, since the amorphous carbon films have a metastable structure, the hybridized carbon structure would be transformed into a more stable state if the energy barrier of the phase transition can be overcome [18]. A consensus was reached that graphite could be converted to hexagonal and cubic diamond at pressures above 15 GPa and temperatures above ~300 K [19]. Since then, many attempts have been made to reduce the difficulty of converting graphite into diamond. Tan et al. [20] investigated the atomic structure, stability, and mechanical properties of the ta-C synthesized under high pressure via *in situ* high-pressure X-ray diffraction and large-scale first-principles calculations, and found the bulk ta-C could be generated by compressing the amorphous carbon with sp^2-C structure at high pressures (97 GPa) and room temperature. Edalati et al. [21] demonstrated that high pressure could thermodynamically stabilize DLC and the formed high-density lattice defects by straining could reduce the energy barrier to DLC formation, which suggested the condition to form DLC from bulk graphite by applying severe plastic deformation under high pressures. Wen and Sun [22] studied the phase transitions of amorphous carbon under both shear strain and pressure via first-principles calculation and found that the shear strain could significantly reduce the external pressure needed to transform from a sp^2-rich structure to a sp^3-rich one. On this basis, Wong et al. [23] showed that hexagonal diamond could be formed from amorphous carbon precursors under pressures ~100 GPa at the relatively low temperature of 400 °C, and the observed distribution of the hexagonal phase was well correlated to regions having the greatest shear strain. A recent study by Dong et al. [24] showed that the graphite could be transformed into ultra-strong sp^3 phases under high pressures with large shearing, and the metastable sp^3 phases transformed into either diamond or graphite upon decompression.

The above-mentioned studies show that pressure can induce sp^2–sp^3 transformation in metastable carbon structure. This phenomenon could also occur during wear of carbon films under the frictional force, and thus affect their performance and applications. However, such studies are very limited. Motivated by such a possibility and potential benefits, we investigated related transformations in metastable

carbon structure under normal loads, tangential loads, and frictional heat during friction/wear processes. It was noticed that the ratio of sp^3/sp^2 in the amorphous carbon films influenced the transformation of sp^2–sp^3 in the metastable carbon structure during the friction process. The sp^3/sp^2 ratio of amorphous carbon film should affect its tribological behavior and applications. Revealing the tribological behavior of amorphous carbon films with different sp^3/sp^2 ratios and elucidating the mechanism for the transformations in the metastable hybridized carbon structures during the friction process would help understand the mechanism and optimize carbon films for effective applications.

Although the transformation from sp^3-C to sp^2-C has been considered as the main factor that is responsible for low COF of amorphous carbon films, it remains a great challenge for understanding the mechanism for the metastable hybridized structural transformation of amorphous carbon under applied pressure and frictional shear stress during a dynamic friction process. In this study, we investigated the tribological performance and the metastable hybridized structural transformation using both experimental techniques and MD simulation. Obtained results of the study would deepen the understanding of the tribological behavior of amorphous carbon films and provide new insight into the transformation of the metastable structures during friction processes.

2 Experimental methods

2.1 Amorphous carbon film deposition

The amorphous carbon film used in this study was deposited on the polished 304 stainless steel disc (φ 60 mm × 5 mm) by ion beam-assisted enhanced unbalanced magnetron sputtering equipment (Diamant-VII-340). Before deposition, the substrate was cleaned by ultrasonic cleaning in an anhydrous ethanol solution to remove surface adsorbed impurities and oil stains. After the substrate was placed into a vacuum chamber, it was further cleaned using argon ions at a bias voltage of –600 V. The base pressure and temperature of the vacuum chamber were maintained at 5 × 10^{-5} Pa and 150 °C during this process, respectively. Ti/TiC transition layers were initially deposited on the substrate to improve the adhesion between the amorphous carbon film and the substrate. A high purity C target (99.99%) was used, and the target current was controlled as 3 A to deposit the amorphous carbon film. The deposition parameters are shown in Table S1 in the Electronic Supplementary Material (ESM).

2.2 Tribological evaluation and wear scar observation

The amorphous carbon film samples and counterparts (balls made of GCr15 of 6 mm in diameter) were ultrasonically cleaned with absolute ethanol for 20 min to remove oil and dirt on the surface, and then dried with a nitrogen flow. The test was performed in vacuum of 1 × 10^{-2} Pa at the temperature of 25 °C with a contact load of 5 N at a sliding speed of 40 rpm (R = 19 mm), using a ball-on-disk vacuum tribometer (Anton Paar, HVTHT). A digital holographic microscope (DHM) with a high-power laser dual-wavelength of 415 and 485 nm (Lyncée Tec, Model R2100) was set during the test to observe the real-time wear scar morphology of the amorphous carbon film during each sliding circle. The apparatus and schematic for the vacuum tribometer with DHM are shown in Fig. 1. Continuous acquisition at the same position was ensured during the test by synchronizing an external trigger with the rotation of the tribometer, and the wear rates of the amorphous carbon film at different sliding circles were calculated using Eq. (1):

$$K = V/(F \cdot S) \tag{1}$$

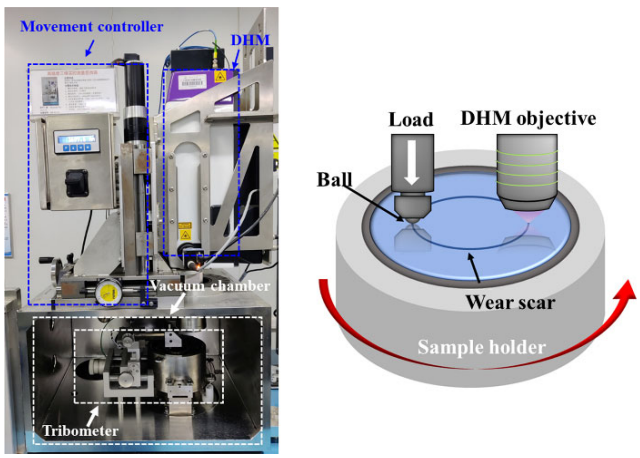

Fig. 1 (a) Apparatus and (b) schematic of the vacuum tribometer with real-time wear scar observation by DHM.

where V is the total loss volume (m^3) of the film caused by wear/friction, F is the contact force (N), and S is the total sliding distance (m).

2.3 Characterization of amorphous carbon film

The bonding information and the sp^3/sp^2 hybridized carbon atoms ratio of the wear scar and the surface of the amorphous carbon film were comparatively acquired by X-ray photoelectron spectroscopy (XPS, Thermo Scientific, ESCALAB 250Xi) and Raman spectrometer (HORIBA, XploRA PLUS).

Based on the site- and material-specific lift-out technique, cross-sectional observation and analysis were conducted for the tribofilm of the amorphous carbon film using a focused ion beam/scanning electron microscope (SEM/FIB, FEI. Helios 5) dual-beam system. Before FIB milling, a Pt layer with a thickness of 10 μm was deposited on the surface of the wear scar to protect the surface layer from being etched away by FIB. Then, an in-time adjustment for ion beam voltage, beam current, and probe size was made to protect the surface integrity and the microstructural features of interest during the FIB milling. Afterward, the microstructure of the tribo-film was observed using a high-resolution transmission electron microscope (HRTEM, Talos F200X).

2.4 MD computational approach

The metastable hybridized amorphous carbon transformation during the friction process was simulated using the Large-scale Atomic/Molecular Parallel Simulation (LAMMPS). The size of the amorphous carbon film model was set to 80 Å × 80 Å × 80 Å. A series of sp^2/sp^3 hybridized atoms (sp^3/sp^2 ratios of the amorphous carbon film models were determined by obtaining the number of C atoms with different coordination numbers using Ovito) of amorphous carbon films of 0.17 (1/5.78), 0.23 (1/4.35), 0.30 (1/3.29), and 0.39 (1/2.57) were settled and randomly filled into the model to make the simulation results have better generalizability. The simulated model was kept at a constant temperature of 300 K for 10 ps and quickly heated to 8,000 K within 10 ps. After staying at the constant temperature for 6 ps, the temperature of the simulated system was cooled promptly to 300 K within 6 ps to obtain a stable amorphous carbon film structure [25]. The carbon atoms were deleted in the top 40 Å part of the model in the Z direction to create a vacuum layer. The simulated model is shown in Fig. S1 in the ESM. The atoms in the fixed layer were not affected by loading, which ensures the stability of the simulation model. The microcanonical ensemble (NVE) was used for the simulation, and the Berendsen method was employed for the thermostat layer to stabilize the temperature at 300 K. Since Tersoff/Zbl potential function has been shown to be suitable for molecular dynamics simulations of the amorphous carbon films [26–28], it was utilized to control the interaction between C atoms in the amorphous carbon films and Fe atoms in the α-Fe counterpart [26]. Specific parameters of the potential function for the modeling are shown in Table 1 [26–28]. The simulated time step was set as 1 fs in this work.

The simulated process contains the stages of relaxation, loading, and sliding friction. In the relaxation stage, the α-Fe counterpart was placed 20 Å above the surface of the amorphous carbon film to avoid the interaction between the amorphous carbon films and the α-Fe counterpart. The entire simulated model was then relaxed for 40 ps to ensure that the simulation system reached stability. In the loading stage, a force of 160 nN was applied to the α-Fe counterpart, which was pressed onto the surface of the amorphous carbon films within 40 ps. In the friction stage, based on the loading force, the α-Fe counterpart was given a speed (v = 60 m/s) along the positive X direction within a reasonable range [29, 30]. Finally, slide the α-Fe counterpart out of the model and then enter the model from the starting end as a

Table 1 Parameters between C and Fe atoms in the Tersoff/Zbl potential function [26–28]. Reproduced with permission from Ref. [26], © American Institute of Physics, 1984; Ref. [27], © IOP Publishing Ltd., 2007; Ref. [28], © IOP Publishing Ltd., 2013.

Bond	D_0 (eV)	r_0 (Å)	R (Å)	D (Å)	S	γ	c	d	h	β (Å^{-1})
C–C	6	1.39	1.85	0.15	1.22	2.08×10^{-4}	330	3.5	1	2.1
Fe–Fe	1.5	2.29	3.15	0.2	2.07	1.16×10^{-2}	1.29	0.34	–0.26	1.4
C–Fe	3.95	1.53	2.6	0.2	1.43	7.49×10^{-2}	1.12	0.95	–0.19	1.82

friction circle, and the total friction simulation process had 40 circles.

3 Experimental results

3.1 Tribological performance

Figure 2 shows the coefficient of friction (COF) curve, wear rate, and the typical wear scar morphology of the amorphous carbon film. It can be seen from Fig. 2(a) that the first 10th sliding circles were in the running-in stage, which showed a high COF and relatively large fluctuations. In the initial stage or running-in stage, the surface irregularities such as roughness and adsorbed layer containing oxygen or oxide [31] may make the amorphous carbon film subjected to three-body wear with formed furrows, resulting in large fluctuation in COF. After a short period of friction, the counterpart started being in direct contact with the amorphous carbon films, and the graphitization was gradually developed at the contact interface, which more or less helped reduce COF. After the first 10 circles, the running-in stage could be considered to be ended, and the COF of the film decreased and became stable with an average COF value of 0.142 within the 10–1,000th friction circles. The inserted figures in Fig. 2(a) illustrate typical wear scar morphologies. The amorphous carbon film acquired a deep and wide wear scar during the running-in stage and gradually worsened during subsequent steady-state wear process.

Figure 2(b) shows the average wear rate of amorphous carbon films as a function of the sliding or friction circles. The average wear rate was determined by measuring the dimensions of 2D profiles in five different locations of the wear track for each case, from which the volume loss per sliding distance and per unit contact force ($m^3/(N·m)$) was calculated as the wear rate. As the friction circle increased from 10th to 1,000th, the wear rate of the amorphous carbon film decreased from 88.5×10^{-14} to 0.9×10^{-14} $m^3/(N·m)$. As shown in Eq. (1), the wear rate was related to the sliding distance, and the wear rate decreased with increasing the sliding distance. This result is consistent with the variation in the wear scar illustrated in Fig. 2(a). Typical wear scar morphologies in different wear stages are illustrated in Fig. 2(c). As shown, the depth of wear scar reached 656.1 nm in the running-in stage. With increasing the sliding distance, the depth of the wear scar increased

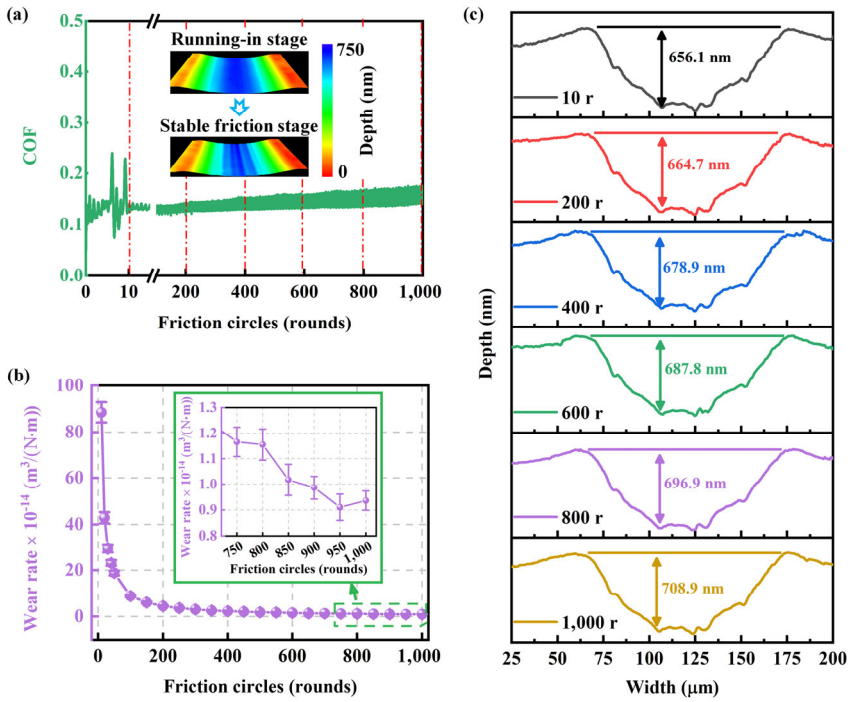

Fig. 2 (a) COF curve of the amorphous carbon film; (b) wear rates of amorphous carbon film with the sliding or friction circles; and (c) changes in the wear scar morphology.

to 664.7 nm at 200th circles. After stable friction for a certain period, the wear scar depth was 678.9 nm at 400 circles, and this value slowly increased to 708.9 nm at 1,000th circles. The optical image and the Raman spectra of the counterpart surface after friction/wear are displayed in Fig. S2 in the ESM, showing that no significant large-area carbon transfer was generated in the central area of the amorphous carbon film in contact with the counterpart after friction but a small amount of transfer was observed at the edge of the contact area.

3.2 Metastable structure transformation

In order to clarify the mechanism for the metastable structure transformation, the wear scar and the surface of the amorphous carbon film were characterized in comparison via XPS, Raman, and HRTEM analysis.

The XPS C1s spectra of the surface and its wear scar of the amorphous carbon film were acquired to quantify the conversion of bonding structures caused by friction. Obtained data and results of the Gaussian fitting analysis are shown in Fig. 3(a). The XPS pattern could be fitted to 3 distinct peaks for the amorphous carbon film. The strong binding energy peak at 285.1 eV corresponds to the C–C bond, the high binding energy peak at 278.1 eV belongs to the C–O bond, and the binding energy peak at 288.9 eV is related to the C=O bond. The formation of C–O and C=O bonds was probably caused by residual water vapor and oxygen molecules during the film deposition and processes. Further analysis by Gaussian fitting of the strong peak of C–C bond binding energy includes two peaks: sp^2-C peak and sp^3-C peak, and the ratio of the carbon atom hybridization bonds is estimated by the peak area ratio.

As shown in XPS spectra, the C 1s core position (284.6 eV) of the wear scar is closer to that of the typical graphite peak (284.3 eV), compared to that of the surface (284.8 eV) of the amorphous carbon film. The deconvolution of the XPS spectrum from wear scar revealed an increased fraction of sp^2-C hybridized bonds (Area of sp^2-C peak is 44,933.1 cps*eV) and a decreased fraction of sp^3 carbon bonds (Area of sp^3-C peak is 15,613.8 cps*eV), compared to the situation of unworn surface of the amorphous carbon film. Besides, the ratio of sp^3-C to sp^2-C hybridized bonds of the film decreased from 1/2.45 to 1/2.87 after friction/wear. Therefore, it can be speculated that the sp^3-C bonds were condensed and converted into sp^2-C bonds during friction due to the fact that sp^2-C bonds are more thermodynamically stable [32]. Meanwhile, the results show that graphitization also has a contribution to the low COF of the amorphous carbon film.

Raman spectroscopy is an effective and non-destructive method to characterize detailed bonding structure of amorphous carbon film. The full spectra of the surface and the wear scar of the film are illustrated in Fig. 3(b). As shown, the broad peak in the range of 800–2,000 cm^{-1} was fitted by the Gaussian function, which could get the D peak near 1,300–1,380 cm^{-1} and the G peak near 1,520–1,580 cm^{-1} [33]. The G peak is generated by the stretching motion of all sp^2-C atom pairs in the carbon ring or long chain, and the D peak is caused by the breathing vibration mode of the sp^2-C atom in the carbon ring. Typically,

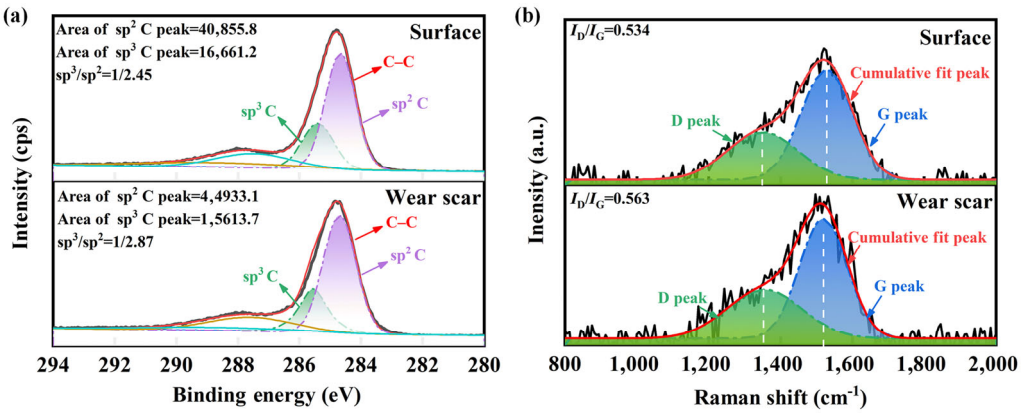

Fig. 3 (a) XPS and (b) Raman spectrum of the amorphous carbon film before and after friction.

the increased integrated intensity ratio of I_D/I_G, closely related to the increased content of sp^2-C bonds configured in aromatic rings, is widely used to evaluate the graphitization of the amorphous carbon film [34]. The I_D/I_G ratio of the wear scar is 0.563, higher than that of the film's surface before friction (0.534), indicating that graphitization occurred at the wear scar of the amorphous carbon film. The graphitization phenomenon was caused by the combined action of the shear force generated and the friction flash temperature at the contact interface during the friction process, resulting in the transformation of hybridized sp^3-C atoms to hybridized sp^2-C atoms. The graphitization phenomenon indicates that hybridized sp^2-C atoms increased at the wear scar position, consistent with the XPS results. The graphitization phenomenon at the wear scar could reduce the shear strength of the contact interface, thereby reducing the COF. As shown in Fig. 2(a), there is a running-in stage with large fluctuation in COF during 0–10 friction circles. After 10 friction circles, the COF fluctuations are significantly lower and COF actually decreases as well, which could be attributed to graphitization of the friction contact area of the amorphous carbon films. As for the later somewhat rise in COF at higher numbers of circles in the stable friction stage, it is attributed to the increased contact between the film and counterpart with deeper and wider wear scar, which increases the resistance to the sliding of the counterpart on the film.

The XPS and Raman characterization demonstrated that the metastable hybridized carbon atoms in amorphous carbon film transformed from hybridized sp^3-C structure to hybridized sp^2-C structure during the friction process. In order to further determine the structural characteristics of the amorphous carbon film, the cross-sectional structure of the wear scar was characterized by a combination of FIB and HRTEM. As displayed in Fig. 4(a), with the assistance of FIB, the specific site of the cross-section of amorphous carbon film along the friction direction in the middle of the wear scar was selected and lifted out by an EasyLift nanomanipulator. The lamella sample was extracted by means of ion bombardment, as shown in Fig. 4(b). An approximate rectangle-shaped morphology can be observed, and the middle region is the thinnest. The presence of the approximate rectangle-shaped morphology was caused by a difference in the intensity of ion bombardment. The cross-sectional HRTEM sample in Fig. 4(b) shows that the amorphous carbon film and its Ti/TiC transition layer were deposited on the 304 substrates, and a relatively thicker Pt protective layer was used to cover the wear scar surface layer of the amorphous carbon film. Meanwhile, the area for HRTEM analysis was selected on the top of the amorphous carbon film in the thinnest area, as observed in Fig. 4(c).

The amorphous carbon structure (subsurface layer of the film), the wear scar layer, and the Pt protective layer are marked as A1, A2, and A3 in Fig. 4(c). Fast Fourier transform (FFT) images and enlarged representative microstructure of zones marked by squares are displayed in Fig. 4(d)–4(f), respectively. As shown in Fig. 4(d) and its inserted figure illustrate, the microstructure of the film's subsurface layer has a typical disordered amorphous carbon structure. During the friction process, some localized ordered nanoclusters formed in the amorphous structure at the worn surface of the film, as shown in Fig. 4(e).

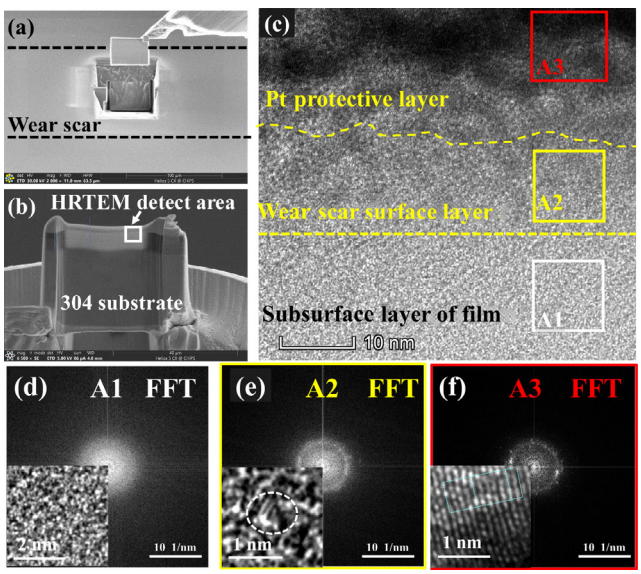

Fig. 4 (a) Cross-sectional HRTEM sample lifted out by an EasyLift nanomanipulator. (b) SEM images of the cross-sectional HRTEM samples after the final thinning. (c) HRTEM image of the amorphous carbon film after friction. (d–f) FFT images of the marked square regions in the corresponding HRTEM image in (c) (The inserted figures in (d–f) are the typically enlarged microstructures in each marked square region.).

The lattice spacing of the localized ordered structure in the wear scar surface layer was determined as 0.204 nm from the inserted figure in Fig. 4(e). Chen et al. [35] studied clustering and local ordering of sp^2-C phase in the outer-most ~3 nm region of central scar surface, and demonstrated that a graphitized tribolayer could be formed due to the shear-induced transformation from sp^3-C to sp^2-C in a superlubricity a-C: H film. Along with the structural characterization Data (XPS and Raman results shown in Fig. 3) and previous studies [36, 37], it can be inferred that the localized ordered structure with lattice spacings of 0.204 nm may be the {101} planes of graphite-2H, which has a positive effect on reducing the COF to a certain extent. From Fig. 4(c), one may also observe that a small number of platinum crystals sputtered into the amorphous carbon structure. In order to distinguish the localized ordered structure in amorphous carbon films from Pt nanoparticles, we analyzed the FFT image and representative local microstructure in the zones marked by squares in the HRTEM image as shown in Fig. 4(f). It can be easily identified that the lattice spacing of the Pt nanostructure is 0.226 ± 0.006 nm, which is its {111} planes.

3.3 MD simulation of friction process

In order to better understand the experimental results and gain insights into the atomistic processes of metastable hybridized amorphous carbon transformation, MD simulations were performed. Figure S3 in the ESM shows the atomic structure of the amorphous carbon films with different sp^3/sp^2. From Figs. S3(a) and S3(c) in the ESM, one may see that the amorphous carbon films with different sp^3/sp^2 ratios are composed of C atoms in three hybridized modes (sp^1-C, sp^2-C, and sp^3-C). The hybridized sp^1-C atoms are mainly distributed on the surface of the amorphous carbon films due to the small coordinated number of C atoms located on the surface of the films. As shown in Figs. S3(b) and S3(d) in the ESM, the hybridized sp^3-C atoms in the film with a sp^3/sp^2 ratio of 1/5.78 are dispersed in the clusters composed of the hybridized sp^2-C atoms, while with the increased sp^3/sp^2 ratio, the skeleton of the amorphous carbon is mainly composed of hybridized sp^3-C atoms in the film with sp^3/sp^2 ratio of 1/2.57. The hybridized sp^2-C atoms existed in the sp^3-C skeleton in the form of short-chain clusters. As the compressive yield strength of sp^3-C bond is higher than that of sp^2-C bond, the amorphous carbon film with high hybridized sp^3-C atoms content shows a better compression strength [38, 39]. Therefore, it could be inferred that the deformation of the amorphous carbon film with a high sp^3/sp^2 ratio is minor, which reduces wear in the running-in stage with decreased contact area and adhesion between the grinding pair and the films.

Figure 5 illustrates curves of the frictional forces and wear rates of the amorphous carbon films with different sp^3/sp^2 ratios as a function of the friction circles, respectively. Figure 5(a) displays that the frictional forces of the amorphous carbon films

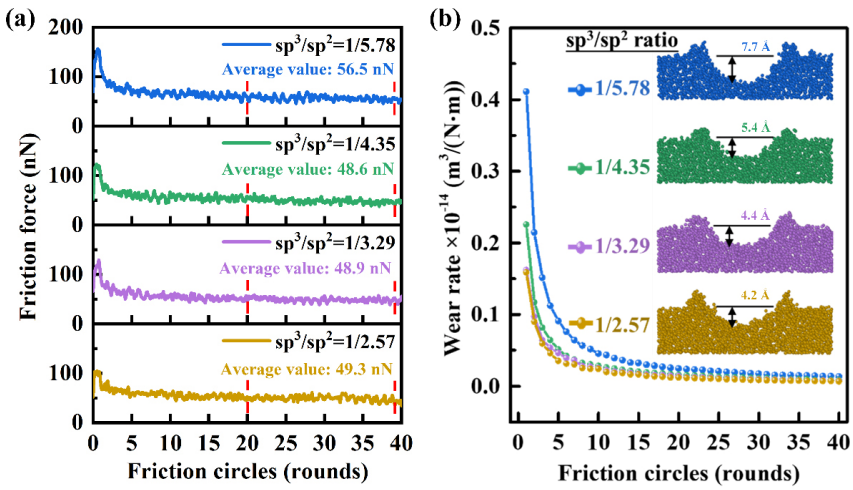

Fig. 5 (a) Frictional forces and (b) wear rates of the amorphous carbon films with different sp^3/sp^2 ratios.

exhibit a significantly high level at the beginning of the friction circles (friction circles < 5th) and then decrease to a relatively low level as friction process proceeds. The average frictional forces of the amorphous carbon films for 20–40th friction circles were calculated. The calculation shows that the average frictional force is 56.523 nN in the film with a sp^3/sp^2 ratio of 1/5.78, and this value decreases to less than 50 nN with increasing the sp^3/sp^2 ratio. Closer observation reveals that the changes in the frictional forces are relatively insignificant when the sp^3/sp^2 ratio of the films increases from 1/4.35 to 1/2.57, showing that the frictional forces are nonlinearly related to the films with different sp^3/sp^2 ratios.

For the wear rate calculation, variations in position of C atoms in the amorphous carbon film during each friction circle were determined using the Ovito software, from which the wear scar maps were drawn. Based on the wear scar dimensions determined via the Origin software, the wear rates of the amorphous carbon films were calculated. As shown in Fig. 5(b), the trend of changes in the simulated wear rates is highly consistent with the experimental result. The wear rates of the amorphous carbon films decrease with increasing friction circles, indicating that the relationship between the wear rate and friction circles is not linear. The film with a lower sp3/sp2 ratio has a higher wear rate. The inserted figures in Fig. 5(b) also illustrate the variations in the wear scar depth of amorphous carbon films with different sp3/sp2 ratios after 40th friction circles. It can be seen that the depth of the wear scar decreases with increasing the sp^3/sp^2 ratio in the amorphous carbon films, which is attributed to the structural features of the films. It is thus necessary to clarify how the metastable hybridized amorphous carbon transforms during friction.

3.4 Mechanism for metastable hybridized amorphous carbon transformation

Figure 6 shows the cross-sectional morphologies of the wear scars on the amorphous carbon films with different sp^3/sp^2 ratios, covering 1st to 40th circles. The friction process shows three stages. The wear scar morphology changes significantly during the 1st friction circle with chip formation. Changes in wear morphology were relatively small during 2nd–5th friction circles, After the 5th friction circle, the change in the wear scar morphology was not obvious. Thus, we chose the wear morphologies of 1, 2, 5, 20, and 40 friction circles as representative morphologies of wear track on the film for the three stages.

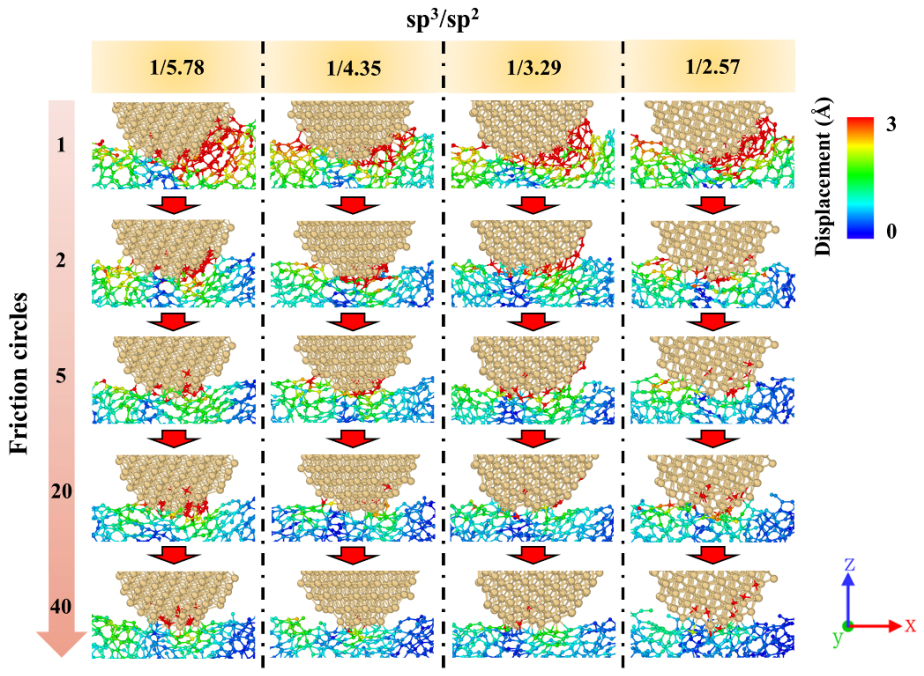

Fig. 6 Morphologies of the amorphous carbon films with different sp^3/sp^2 ratios along the cross-section of the wear scar during the friction process.

In the initial stage of friction (first friction circle), the large displacements of C atoms and their intensive accumulations in front of the counterpart suggest the bond breakage and thus the chip formation during the initial abrasive wear. The worn surface of the amorphous carbon films is subjected to plowing in the early stage of the friction/wear process. However, when the number of friction circles increases, C atoms mainly follow the tail of the α-Fe counterpart, indicating that the wear mode of the amorphous carbon films changes from abrasive wear to a mixture of abrasion and adhesive wear. An optical image of the counterpart surface after friction and corresponding Raman spectra show that a small amount of transferred amorphous carbon was detected at the edge of the worn area of the counterpart (Fig. S2 in the ESM). As shown in Fig. 6, the displacement becomes smaller with increasing the sp^3/sp^2 ratio (more blue sites), meaning that the adhesive wear could be more obvious when carbon atoms in the film have a low sp^3/sp^2 ratio. For more quantitative information, the interfacial bond numbers of the amorphous carbon films with different sp^3/sp^2 ratios are provided in Fig. S4 in the ESM. As shown in Fig. S4, in general, the interfacial C–Fe bond number is dynamically decreased with an increase in the sp^3/sp^2 ratio, which is consistent with the observations shown in Fig. 6. One may see in Fig. 5 that with the increase in the sp^3/sp^2 ratio, the wear scar depth of the amorphous carbon films decreases significantly, suggesting that higher sp^3/sp^2 ratios benefit the wear resistance of the amorphous carbon films.

Although the MD simulation was performed for small systems on a nano-scale to elucidate underlying mechanisms rather than to obtain quantitatively accurate data comparable to the realistic situation, the changes in COF curves, wear rate, and wear morphology obtained from the experiments are basically consistent with those from the MD simulations. Therefore, it is reasonable to further explore the transformation mechanism of the interfacial structure of amorphous carbon films during friction by MD simulations.

Although the results in Fig. 6 and the reported studies in the literature [40] show that the bonds at the contact interface between the films and their counterparts are broken easily, the metastable transformation of the hybridized amorphous carbon is unclear. Figure S5 in the ESM illustrates metastable hybridized structure transformation in the amorphous carbon films with different sp^3/sp^2 ratios during the friction process. The curves of each hybridized structure fluctuate with increased friction circles. The statistic information on transformation in the whole amorphous carbon film model during the initial state, running-in state, and steady wear state of the friction process is generalized and comparatively analyzed in Fig. 7. During the friction process, the proportion of hybridized sp^2-C atoms in the amorphous carbon films increases to various degrees because of different sp^3/sp^2 ratios, which indicates that the graphitization may occur at the wear scar in the amorphous carbon film whatever the sp^3/sp^2 ratio is. It is well known that the existence of graphitization in amorphous carbon films reduces COF during the friction process [33]. It can be noticed that the increment of hybridized sp^2-C atoms differs, depending on the film's sp^3/sp^2 ratio, and higher sp^3/sp^2 ratios could lead to more graphitization during the friction process. Nevertheless, the proportion of hybridized sp^3-C atoms in the amorphous carbon films changes differently in the film with different sp^3/sp^2 ratios during the friction process.

It is observed that sp^1-C atoms are mainly distributed on the surface of the amorphous carbon films. The proportion of sp^1-C atoms markedly decreases in films with higher sp^3/sp^2 ratios. Besides, the proportion of sp^1-C atoms decreases significantly during friction, generating more sp^2-C atoms but reducing sp^3-C atoms as Fig. 7 illustrates. Such a trend is more obvious for films with higher sp^3/sp^2 ratios, which suggests that in films with higher sp^3/sp^2 ratios favor the transformation of sp^1-C and sp^3-C atoms to sp^2-C atoms during the friction process.As shown in Figs. 7(a) and 7(b), one may see that the proportion of hybridized sp^3-C atoms in the amorphous carbon films with the sp^3/sp^2 ratios of 1/5.78 and 1/4.35 does not decrease but slightly increase during the friction process. More notably, the proportion of hybridized sp^3-C atoms does not gradually increase during the friction process but shows a significant increase in the initial running-in state. Afterwards, it changes to a relatively lower level as the friction continues after the 20th

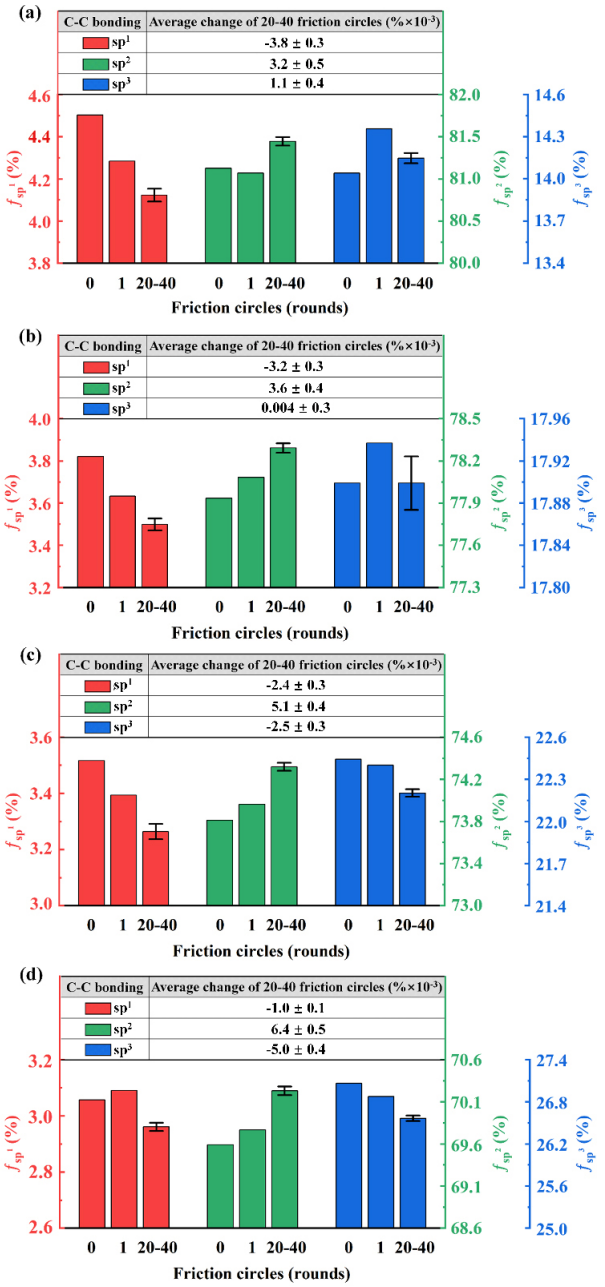

Fig. 7 (a)–(d) Proportion of hybridized amorphous carbon atoms in the films with sp^3/sp^2 ratios equal to 1/5.78, 1/4.35, 1/3.29, and 1/2.57, respectively.

friction circles. The metastable transformation of hybridized amorphous carbon from sp^2-C type to sp^3-C type during the friction process could be induced by the external force. It was reported that the pressure could induce the transformation from the sp^2-C structure to the sp^3-C structure, shown by an experimental study [41] and first-principles calculations [42]. Meanwhile, a recent study also revealed that the shear strain could effectively induce the transformation of hybridized sp^3-C structure in amorphous carbon under much lower pressure [22]. Although the metastable hybridized sp^3-C structure could be short-lived and transformed from unsaturated sp^1-C and sp^2-C structures under an applied contact force during the friction/wear process, it is not easy to maintain the state. The reformed hybridized structures may revert from sp^3-C type to the more stable hybridized sp^2-C type with the generated graphitization at the contact interface during friction. Besides, the hybridized sp^1-C atoms from the film's surface also play an essential role in the hybridized sp^2-C structure generation in the amorphous carbon films with low sp^3/sp^2 ratios. While the proportion of hybridized sp^3-C atoms in the amorphous carbon films with sp^3/sp^2 ratios of 1/3.29 and 1/2.57 reveals a gradually decreasing trend during the friction process with a more complex metastable transformation of hybridized sp^1-C atoms, which can be seen in Figs. 7(c) and 7(d).

Figure S5 in the ESM shows the curves of the interfacial C–Fe bonding number of the amorphous carbon films with different sp^3/sp^2 ratios. According to Fig. S5 in the ESM, the interfacial C–Fe bond number decreased significantly as the sp^3/sp^2 ratio increased from 1/5.78 to 1/3.29 during 5–40 friction circles, while it increased when sp^3/sp^2 was equal to 1/2.57. One may see in Fig. 5 that with the increase of sp^3/sp^2 ratio, the wear scar depth of the amorphous carbon films decreases significantly, leading to decreased contact area between the counterpart and the amorphous carbon film. The number of saturated carbon atoms in the amorphous carbon film increases with increasing the sp^3/sp^2 ratio, causing a decreased interfacial C–Fe bonding number. Based on the results shown in Fig. 7, the amorphous carbon film with the sp^3/sp^2 ratio of 1/2.57 has the highest decreasing trend in the saturated carbon atoms at the contact interface during the friction process. However, the wear scar depth of the film with a sp^3/sp^2 ratio of 1/2.57 is not much different from that with sp^3/sp^2 ratio equal to 1/3.29. Moreover, the amorphous carbon film with sp^3/sp^2 equal to 1/2.57 transforms more unsaturated carbon atoms at the contact interface during the friction process; thus, the number of

interfacial C–Fe bonding increased slightly compared with that of the film with sp^3/sp^2 equal to 1/3.29.

It can therefore be inferred that the applied pressure and the frictional shear stress drive the metastable hybridized amorphous carbon transformation by breaking the existing carbon atomic bonds in the amorphous carbon film. The hybridized amorphous carbon could then be reformed into new hybridized structures, depending on the frictional environment. Although the transformation ability of hybridized amorphous carbon from sp^2-C to sp^3-C type is weakened with higher sp^3/sp^2 ratios, it can be concluded that the friction process provides the condition for the inter-transformation of the metastable hybridized amorphous carbon. A schematic diagram showing the transformation possibility of the metastable hybridized amorphous carbon with different sp^3/sp^2 ratios is presented in Fig. 8. More detailed transformation can be found in Fig. S6 in the ESM, showing the bonding transformation from sp1-C to sp^2-C and sp^3-C, respectively, during wear/friction of the metastable hybridized amorphous carbon films with low and high sp^3/sp^2 ratios. As shown in Fig. S6 in the ESM, the transformation of the metastable hybridized amorphous carbon is mainly due to the frictional force. In the loading stage, the structure of the metastable hybridized amorphous carbon is transformed under the frictional shear stress and pressure.

Radial distribution function (RDF, g(r)) is an important structural characteristic of amorphous materials, which can be determined using Eq. (2) [43]:

$$g(r)=\frac{1}{\rho 4\pi r^2\delta r}\frac{\sum_{I\text{-}1}^{T}\sum_{I\text{-}1}^{N}\Delta N(r\to r+\delta_r)}{NT}-\frac{\mathrm{d}N}{\rho 4\pi r^2\mathrm{d}r} \quad (2)$$

where ρ is the average density of the system, δr is the distance difference, T is the total time, N is the total number of atoms, and dN is the number of molecules between $r \to r + \delta r$. Figure 9 illustrates RDF curves of the amorphous carbon films with different sp^3/sp^2 ratios before and after friction. As observed, the first peak near 1.54 Å in the RDF curve is related to the bond length of the amorphous structure, and the second peak near 2.52 Å is associated with the bond length and bond angle of the amorphous structure. Besides, a small peak at 2.1 Å is caused by the truncation

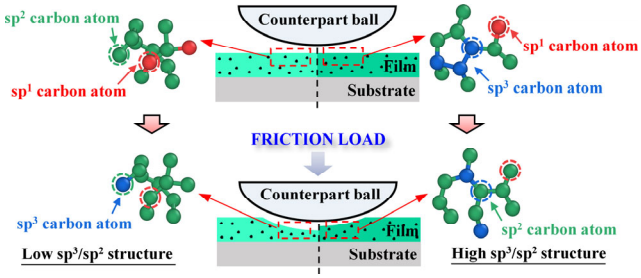

Fig. 8 Schematic diagram of the transformation possibility of the metastable hybridized amorphous carbon with low and high sp^3/sp^2 ratios, respectively.

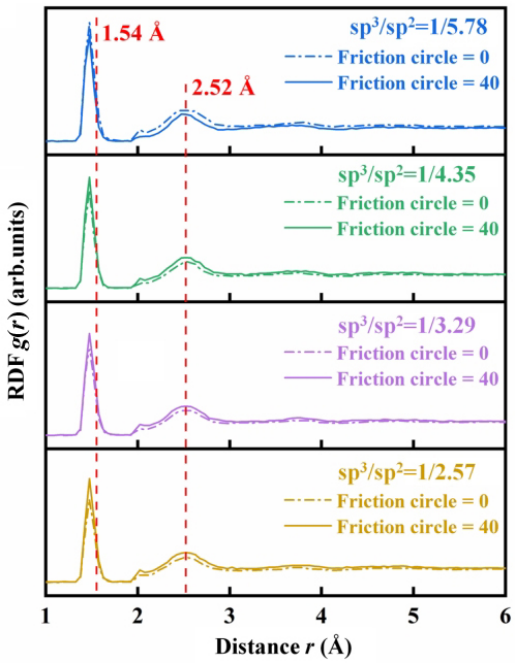

Fig. 9 RDF curves of the amorphous carbon films with different sp^3/sp^2 ratios before and after friction.

of the Tersoff-type potential function and can be considered a "false peak" [43]. The results demonstrate that the amorphous carbon films with different sp^3/sp^2 ratios have both short-range order and long-range disorder structural characteristics, and their RDF curves are changed significantly by friction. The RDF curves of the amorphous carbon films with sp^3/sp^2 ratios from 4.35 to 2.57 show a downward shift at the location of wear scars. However, the RDF curves of the amorphous carbon film with a sp^3/sp^2 ratio of 1/5.78 reveal an opposite trend.

In order to further investigate the degree of structural disorder of the amorphous carbon films, the translation order parameters (t) of the films with different sp^3/sp^2 ratios before and after friction are

calculated using Eq. (3) [44, 45]:

$$t = \frac{\int_0^{\xi_c} |g(\xi) - 1| \mathrm{d}\xi}{\xi_c} \quad (3)$$

where $\xi(= r\rho^{1/3})$ is the distance between carbon atoms, r is what divided by the mean separation between carbon atoms at the given density, ρ is the density or the number of molecules per unit volume (N/V), g is the carbon–carbon radial distribution function, and ξ_c is a cut-off distance. The value of ξ_c is set as 1.85 Å in this work according to the cut-off distance for C–C bond [45]. In an ideal gas, $g = 1$, and t vanishes. While in a crystal, t is large, since there is long-range translational order and $g \neq 1$ over a long distance.

As shown in Fig. 10, as the sp^3/sp^2 ratio of the amorphous carbon films increases, the translation order parameter t gradually decreases, indicating that the degree of structural disordering of the amorphous carbon films increases. After friction, except for the translation order parameter t of the amorphous carbon film with a low sp^3/sp^2 ratio of 1/5.78 decreases, those with sp^3/sp^2 ratios from 1/4.35 to 1/2.57 show an increasing trend. The high sp^3/sp^2 ratio leads to an increased structural ordering at the wear scar. In comparison, the translation order parameter t has an opposite trend for the amorphous carbon film with a low sp^3/sp^2 ratio of 1/5.78, indicating a structural disorder at the wear scar. According to Figs. 7 and 10, the proportions of both sp^2-C and sp^3-C increased in the amorphous carbon films with sp^3/sp^2 = 1/5.78 after friction/wear, while only the proportion of sp^3-C atoms increased and those of sp^2-C and sp^1-C decreased or remained almost unchanged in the amorphous carbon films with other sp^3/sp^2 ratios after friction/wear.

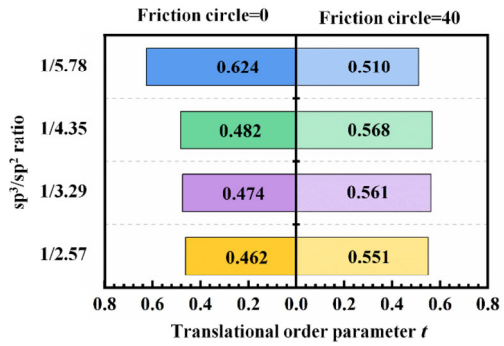

Fig. 10 Translational order parameter t of the amorphous carbon films with different sp^3/sp^2 ratios before and after friction.

This indicates that the structural ordering of the contact interface of the amorphous carbon films increases significantly only when the proportion of C atoms in a single hybridized mode increases during the friction process (e.g. the proportion of sp^2 hybridized C atoms increases, and the proportion of sp^1 and sp^2 hybridized C atoms decreases or remains unchanged), while the structural ordering of the contact interface of the amorphous carbon films decreases when the proportion of C atoms in multiple hybridized modes increases (e.g. the proportion of sp^2 and sp^3 hybridized C atoms increases, and the proportion of sp^1 hybridized C atoms decreases).

4 Conclusions

The metastable hybridized structure transformation in amorphous carbon film during the friction process was investigated. Both experiments and molecular dynamics (MD) simulation showed that the wear mode of the film changed from abrasive wear to a mixture of abrasion and adhesive wear, causing a rapid decrease in the wear rate after the running-in stage. The hybridized amorphous carbon structure is not permanently transformed from sp^3-C to sp^2-C type at the beginning of the friction process, which is a dynamic metastable transformation. It is demonstrated that the ratio of sp^3/sp^2 in the amorphous carbon films influenced the transformation of sp^2–sp^3 in the metastable carbon structure during the friction/wear process. The amorphous carbon films with higher sp^2-C proportions reveal the transformation from sp^2-C to sp^3-C under pressure and shear stress. However, the formed sp^3-C atoms could be short-lived and may gradually transform to sp^2-C ones with graphitization at the contact interface of the films. The amorphous carbon films with high sp^3-C ratio tend to transform from sp^3-C to sp^2-C with increased degree of ordering. It can be concluded that the inter-transformation of the metastable hybridized amorphous carbon occurs by breaking the existing carbon atomic bonds and reforming new hybridized structures. The radial distribution function and translational order parameter indicate that the high sp^3/sp^2 ratio may lead to increased structural ordering at the wear scar after friction. This study clarifies the mechanism for the metastable hybridized carbon

structure transformation during the friction/wear process, which helps understand the mechanism for the dynamic transformation in the amorphous carbon film caused by friction.

Acknowledgements

This work was co-supported by the National Natural Science Foundation of China (No. 51905466), Aeronautical Science Foundation of China (No. 201945099002), Natural Science Foundation of Hebei Province, China (Nos. E2021203191 and E2020203184), and Youth Top Talent Project of Hebei Province Higher Education, China (No. BJ2019058).

Declaration of competing interest

The authors have no competing interests to declare that are relevant to the content of this article.

Electronic Supplementary Material: Supplementary material is available in the online version of this article at https://doi.org/10.1007/s40544-022-0690-x.

Open Access This article is licensed under a Creative Commons Attribution 4.0 International License, which permits use, sharing, adaptation, distribution and reproduction in any medium or format, as long as you give appropriate credit to the original author(s) and the source, provide a link to the Creative Commons licence, and indicate if changes were made.

The images or other third party material in this article are included in the article's Creative Commons licence, unless indicated otherwise in a credit line to the material. If material is not included in the article's Creative Commons licence and your intended use is not permitted by statutory regulation or exceeds the permitted use, you will need to obtain permission directly from the copyright holder.

To view a copy of this licence, visit http://creativecommons.org/licenses/by/4.0/.

References

[1] Holmberg K, Erdemir A. Influence of tribology on global energy consumption, costs and emissions. *Friction* **5**(3): 263–284 (2017)

[2] Khadem M, Penkov O V, Yang H K, Kim D E. Tribology of multilayer coatings for wear reduction: A review. *Friction* **5**(3): 248–262 (2017)

[3] Meng Y, Xu J, Jin Z, Prakash B, Hu Y. A review of recent advances in tribology. *Friction* **8**(2): 221–300 (2020)

[4] Tyagi A, Walia R S, Murtaza Q, Pandey S M, Tyagi P K, Bajaj B. A critical review of diamond like carbon coating for wear resistance applications. *Int J Refract Hard Met* **78**: 107–122 (2019)

[5] Khamseh S, Alibakhshi E, Ramezanzadeh B, Sari M G, Nezhad A K. Developing a graphite like carbon: niobium thin film on GTD-450 stainless steel substrate. *Appl Surf Sci* **511**: 145613 (2020)

[6] Li R, Wang Y, Zhang J, Meyer E. Tribochemistry of ultra-low friction fullerene-like carbon films in humid air. *Appl Surf Sci* **507**: 145040 (2020)

[7] Berman D, Narayanan B, Cherukara M J, Sankaranarayanan S K R S, Erdemir A, Zinovev A, Sumant A V. Operando tribochemical formation of onion-like-carbon leads to macroscale superlubricity. *Nat Commun* **9**(1): 1–9 (2018)

[8] Al Mahmud K A H, Kalam M A, Masjuki H H, Mobarak H M, Zulkifli N W M. An updated overview of diamond-like carbon coating in tribology. *Crit Rev Solid State* **40**(2): 90–118 (2015)

[9] Zeng Q, Eryilmaz O, Erdemir A. Superlubricity of the DLC films-related friction system at elevated temperature. *Rsc Adv* **5**(113): 93147–93154 (2015)

[10] Liu Y, Yu B, Cao Z, Shi P, Zhou N, Zhang B, Zhang J, Qian L. Probing superlubricity stability of hydrogenated diamond-like carbon film by varying sliding velocity. *Appl Surf Sci* **439**: 976–982 (2018)

[11] Fan X, Xue Q J, Wang L. Carbon-based solid-liquid lubricating coatings for space applications-A review. *Friction* **3**(3): 191–207 (2015)

[12] Li W, Fan X, Li H, Zhu M, Wang L. Probing carbon-based composite coatings toward high vacuum lubrication application. *Tribol Int* **128**: 386–396 (2018)

[13] Erdemir A, Eryilmaz O L, Fenske G. Synthesis of diamondlike carbon films with superlow friction and wear properties. *J Vac Sci Technol A* **18**(4): 1987–1992 (2000)

[14] Wang K, Zhang J, Ma T, Liu Y, Song A, Chen X, Hu Y, Carick R W, Luo J. Unraveling the friction evolution mechanism of diamond-like carbon film during nanoscale running-in process toward superlubricity. *Small* **17**(1): 2005607 (2021)

[15] Liu H, Tanaka A, Umeda K. The tribological characteristics of diamond-like carbon films at elevated temperatures. *Thin Solid Films* **346**(1–2): 162–168 (1999)

[16] Fan X, Hu Z, Huang W. In-situ TEM studies on stick-slip friction characters of sp^2 nanocrystallited carbon films. *Friction* **10**: 1635–1649 (2022)

[17] Chen X, Zhang C, Kato T, Yang X, Wu S, Wang R, Nosaka M, Luo J. Evolution of tribo-induced interfacial nanostructures governing superlubricity in a-C: H and a-C: H: Si films. *Nat Commun* **8**(1): 1675 (2017)

[18] Aust R B, Drickamer H G. Carbon: A new crystalline phase. *Science* **140**(3568): 817–819 (1963)

[19] Irifune T, Kurio , Sakamoto S, Inoue T, Sumiya H. Ultrahard polycrystalline diamond from graphite. *Nature* **421**(6923): 599–600 (2003)

[20] Tan L, Sheng H, Lou H, Cheng B, Xuan Y, Prakapenka V B, Greenberg E, Zeng Q, Peng F, Zeng Z. High-pressure tetrahedral amorphous carbon synthesized by compressing glassy carbon at room temperature. *J Phys Chem C* **124**(9): 5489–5494 (2020)

[21] Edalati K, Daio T, Ikoma Y, Arita M, Horita Z. Graphite to diamond-like carbon phase transformation by high-pressure torsion. *Appl Phys Lett* **103**(3): 034108 (2013)

[22] Wen L, Sun H. Understanding shear-induced sp^2-to-sp^3 phase transitions in glassy carbon at low pressure using first-principles calculations. *Phys Rev B* **98**(1): 014103 (2018)

[23] Wong S, Shiell T B, Cook B A, Bradby J E, McKenzie D R, McCulloch D G. The shear-driven transformation mechanism from glassy carbon to hexagonal diamond. *Carbon* **142**: 475–481 (2019)

[24] Dong J, Yao Z, Yao M, Li R, Hu K, Zhu L, Wang Y, Sun H, Sundqvist B, Yang K, Liu B. Decompression-induced diamond formation from graphite sheared under pressure. *Phys Rev Lett* **124**(6): 065701 (2020)

[25] Shao W, Zhou Y, Shi Z, Rao L, Hu T, Xing X, Yang Q. Effects of carbide forming elements Me on residual stress and mechanical properties of DLC films by molecular dynamics simulation. *Mater Today Commun* **23**: 100946 (2020)

[26] Berendsen H J C, Postma J P M, Van Gunsteren W F, DiNola A, Haak J R. Molecular dynamics with coupling to an external bath. *J Chem Phys* **81**(8): 3684–3690 (1984)

[27] Müller M, Erhart P, Albe K. Analytic bond-order potential for bcc and fcc iron—Comparison with established embedded-atom method potentials. *J Phys-Condens Mat* **19**(32): 326220 (2007)

[28] Henriksson K O E, Björkas C, Nordlund K. Atomistic simulations of stainless steels: A many-body potential for the Fe–Cr–C system. *J Phys-Condens Mat* **25**(44): 445401 (2013)

[29] Li X, Wang A, Lee K. Mechanism of contact pressure-induced friction at the amorphous carbon/alpha olefin interface. *Npj Comput Mater* **4**(1): 1–9 (2018)

[30] Hayashi K, Tezuka K, Ozawa N, Shimazaki T, Adachi K, Kubo M. Tribochemical reaction dynamics simulation of hydrogen on a diamond-like carbon surface based on tight-binding quantum chemical molecular dynamics. *J Chem Phys C* **115**(46): 22981–22986 (2011)

[31] Shi P, Sun J, Liu Y, Zhang B, Zhang J, Chen L, Qian L. Running-in behavior of a H-DLC/Al_2O_3 pair at the nanoscale. *Friction* **9**(6): 1464–1473 (2021)

[32] Kalish R, Lifshitz Y, Nugent K, Prawer S. Thermal stability and relaxation in diamond-like-carbon. A Raman study of films with different sp^3 fractions (ta-C to a-C). *Appl Phys Rev B* **74**(20): 2936–2938 (1999)

[33] Bai C, Gong Z, An L, Qing L, Zhang J, Yushkov G, Nikolaev A, Shandrikov M, Zhang B. Adhesion and friction performance of DLC/rubber: The influence of plasma pretreatment. *Friction* **9**(3): 627–641 (2021)

[34] Zhou Y, Ma W, Geng J, Wang Q, Rao L, Qian Z, Xing X, Yang Q. Exploring long-run reciprocating wear of diamond-like carbon coatings: microstructural, morphological and tribological evolution. *Surf Coat Technol* **405**: 126581 (2021)

[35] Chen X, Zhang C, Kato T, Yang X, Wu S, Wang R, Nosaka M, Luo J. Evolution of tribo-induced interfacial nanostructures governing superlubricity in a-C: H and a-C: H: Si films. *Nat Commun* **8**(1): 1675 (2017)

[36] Wang D S, Chang S Y, Huang Y C, Wu J B, Lai H J, Leu M S. Nanoscopic observations of stress-induced formation of graphitic nanocrystallites at amorphous carbon surfaces. *Carbon* **74**: 302–311 (2014)

[37] Zhou Y F, Chen Z H, Hu Z H, Li L, Yang Q X, Xing X L. Tribological performance of hydrogenated diamond-like carbon coating deposited on superelastic 60NiTi alloy for aviation self-lubricating spherical plain bearings. *Chinese J Aeronau* **35**(12): 309–320 (2022)

[38] J. Robertson. Diamond-like amorphous carbon. *Mater Sci Eng R* **37**: 129–281 (2002)

[39] Li L, Xu M, Song W, Ovcharenko A, Zhang G, Jia D. The effect of empirical potential functions on modeling of amorphous carbon using molecular dynamics method. *Appl Surf Sci* **286**: 287–297 (2013)

[40] Kunze T, Posselt M, Gemming S, Seifert G, Konicek A R, Carpick R W, Pastewka L, Moseler M. Wear, plasticity, and rehybridization in tetrahedral amorphous carbon. *Tribol Lett* **53**(1): 119–126 (2014)

[41] Hu M, He J L, Zhao Z S, Strobel T A, Hu W T, Yu D L, Sun H, Liu L Y, Li Z H, Ma M D, et al. Compressed glassy carbon: An ultrastrong and elastic interpenetrating graphene network. *Sci Adv* **3**(6): e1603213 (2017)

[42] Hu M, Zhang S S, Liu B, Wu Y J, Luo K, Li Z H, Ma M D, Yu D L, Liu L Y, Gao Y F, et al. Heat-treated glassy carbon

under pressure exhibiting superior hardness, strength and elasticity. *J Mater* **7**(1): 177–184 (2021)

[43] Zhang S, Shao W, Rao L, He Q, Zhou Y, Xing X, Yang Q. Effects of Ti doping on structure and internal stress of amorphous carbon films on the γ-Fe substrate: Molecular dynamics simulation. *Langmuir* **37**(48): 14072–14080 (2021)

[44] Errington J R, Debenedetti P G. Relationship between structural order and the anomalies of liquid water. *Nature* **409**(6818): 318–321 (2021)

[45] Rao L, Liu H, Hu T, Shao W, Shi Z, Xing X, Zhou Y, Yang Q. Relationship between bonding characteristic and thermal property of amorphous carbon structure: Ab initio molecular dynamics study. *Diam Relat Mater* **111**: 108211 (2021)

Yefei ZHOU. He received his Ph.D. degree from Yanshan University. He is an associate professor at School of Mechanical Engineering, Yanshan University, China. He is a visiting scholar at University of Alberta, Canada (2022). His research interests focus on developing self-lubricating films and coatings for mechanical systems at extreme working conditions.

Xiaolei XING. He received his Ph.D. degree from Yanshan University. He is an associate professor at School of Mechanical Engineering, Yanshan University, China. His research interests focus on developing high-strength/toughness coatings for friction mechanisms in complex environments.

Dongyang LI. He received doctor degree in materials physics from University of Science and Technology Beijing, and in metallurgical engineering from McGill University, respectively. He is a professor at Department of Chemical & Materials Engineering, University of Alberta. Dr. Li received MetSoc 2020 Distinguished Materials Scientist Award (the Metallurgy & Materials Society of CIM) and other honors & awards, and has in excess of 420 publications, including 380 refereed journal publications. He is an invited contributor for authoritative handbooks (Elsevier, Springer, and ASM International) in wear and tribology. His interests of research include surfaces and interfaces, wear and corrosion-wear synergy, electron work function-based methodologies for materials design and analysis, and computational materials science.